Lasers in Surgery and Medicine 24:151–166 (1999)

Modeling Laser Treatment of Port Wine Stains With a Computer-Reconstructed Biopsy

T. Joshua Pfefer, MS,[1]* Jennifer Kehlet Barton, PhD,[2] Derek J. Smithies, PhD,[3] Thomas E. Milner, PhD,[1] J. Stuart Nelson, MD, PhD,[3] Martin J. C. van Gemert, PhD,[4] and Ashley J. Welch, PhD[1]

[1]Biomedical Engineering Program, The University of Texas at Austin, Austin, Texas 78712
[2]Biomedical Engineering Program, University of Arizona, Tuscon, Arizona 85724
[3]Beckman Laser Institute and Medical Clinic, University of California, Irvine, California 92715
[4]Laser Center, Academic Medical Center, Amsterdam, 1105 AZ, The Netherlands

Background and Objective: **The efficacy of laser treatment of port wine stains (PWS) has been shown to be highly dependent on patient-specific vasculature. The effect of tissue structure on optical and thermal mechanisms was investigated for different pulse durations by using a novel theoretical model that incorporates tissue morphology reconstructed tomographically from a PWS biopsy.**
Study Design/Materials and Methods: **An optical-thermal numerical model capable of simulating arbitrarily complex, three-dimensional tissue geometries was developed. The model is comprised of (1) a voxel-based Monte Carlo optical model, (2) a finite difference thermal model, and (3) an Arrhenius rate process calculation to predict the distribution of thermal damage. Simulations based on previous computer-based reconstruction of a series of 6 μm sections from a PWS biopsy were performed for laser pulse durations (τ_p) of 0.5, 5.0, and 10.0 ms at a wavelength of 585 nm.**
Results: **Energy deposition rate in the blood vessels was primarily a function of vessel depth in skin, although shading effects were evident. Thermal confinement and selectivity of damage were seen to be inversely proportional to pulse duration. The model predicted blood-specific damage for τ_p = 0.5 ms, vascular and perivascular damage for τ_p = 5 ms, and widespread damage in superficial regions for τ_p = 10 ms. The effect of energy deposition in the epidermis was most pronounced for longer pulse durations, resulting in increased temperature and extent of damage.**

Contract grant sponsor: Office of Naval Research Free Electron Laser Biomedical Science Program; Contract grant number: N00014-91-J-1564; Contract grant sponsor: Albert W. and Clemmie A. Caster Foundation; Contract grant sponsor: Whitaker Foundation; Contract grant number: WF-21025; Contract grant sponsor: National Institute of Health; Contract grant number: R01AR43419.

*Correspondence to: T. Joshua Pfefer, Biomedical Engineering Program, ENS 610, The University of Texas at Austin, Austin, TX 78712. E-mail: pfefer@ccwf.cc.utexas.edu

Accepted 22 September 1998

Conclusion: **Pulse durations between 0.5 and 5 ms are likely optimal for the PWS analyzed. The incorporation of a tomographically reconstructed PWS biopsy into an optical-thermal model represents a significant advance in numerical modeling of laser-tissue interaction. Lasers Surg. Med. 24:151–166, 1999.**

Key words: finite difference; heat transfer; light propagation; Monte Carlo; numerical modeling; pulse duration; thermal damage; tissue reconstruction

INTRODUCTION

Investigations of laser treatment of port wine stains (PWS) — a vascular condition resulting from an overabundance and/or enlargement of dermal capillaries [1] — have clarified many aspects of treatment, although clinical results are still highly variable [2,3]. The pulsed dye laser parameters most commonly used in clinical treatment of vascular lesions are a wavelength (λ) of 585 nm, beam diameter (D) of 5–10 mm (the maximum possible with current technology), pulse duration (τ_p) of approximately 450 μs, and radiant exposure of 3–10 J/cm^2 [2,4] These values may not represent the optimal laser parameters; for example, improvement in the outcome of PWS treatment has been reported for pulse durations of 1 ms or greater [3,5].

Theoretical models have helped to explain the relevant laser-tissue interaction mechanisms that determine the effectiveness of selective photothermolysis. The successful results obtained by using λ = 585 nm are due to the combination of low absorption in epidermis and dermis and moderately high absorption by oxy- and deoxyhemoglobin. This allows deeper penetration depth and more constant energy deposition across individual vessels than wavelengths such as 577 nm, yet maintains selectivity of absorption [6,7]. Increasing beam diameter for a constant radiant exposure leads to increased fluence at greater depths due to diffusive light scattering effects [8,9]. Modeling has identified potential techniques for improving treatment of vascular lesions. Pulse durations of 1–10 ms, or values corresponding to the thermal relaxation time of targeted vessels, may substantially improve treatment [10–12].

Modeling of Light Propagation

Previous theoretical studies of PWS laser treatment have generally employed assumptions that have led to "grossly simplified" models [12]. Common assumptions regarding light propagation have included uniform distribution of energy across a vessel [12], the application of Beer's law to a scattering medium [8], and the use of highly idealized geometry [13]. The most rigorous optical models of PWS treatment have simulated the propagation and absorption of light in skin using the Monte Carlo method [14]. In these studies, skin morphology has been represented as a wholly homogeneous layer [15], a succession of homogeneous layers [16–18], layers with a single cylindrical vessel [9,15,19], or layers with arrays of cylindrical vessels [20–22].

Recently, we have developed a voxel-based Monte Carlo model named MAGNUM (Modular Adaptable Grid Numerical Model), which can simulate arbitrarily complex three-dimensional heterogeneous tissue morphology [23]. MAGNUM has been used to simulate dermal vasculature based on optical coherence tomography (OCT) images [23,24] and a sequence of histological sections [25]. We note that similar techniques have been investigated for other biomedical optics applications such as element-based, dynamic optical-thermal modeling [26] and simulation of photon migration using the transport equation in conjunction with image-defined geometry [27].

Modeling of Heat Transfer and Thermal Damage

Thermal models of photothermolysis are commonly based on simplifications such as instantaneous energy depositon and temperature rise [13,28] and thermal damage endpoints involving a threshold temperature over a specific region [18,29]. Thermal modeling and bioheat transfer techniques alleviate the need for these potentially inaccurate assumptions. The most advanced PWS thermal models have used the finite-difference technique to account for arbitrary laser pulse duration and heat conduction yet have used either threshold temperatures for damage prediction [10,29] or layered geometry [18]. Improved realism in simulation of thermal damage accumulation is obtained by using the Arrhenius rate process relation, which describes damage as a linear

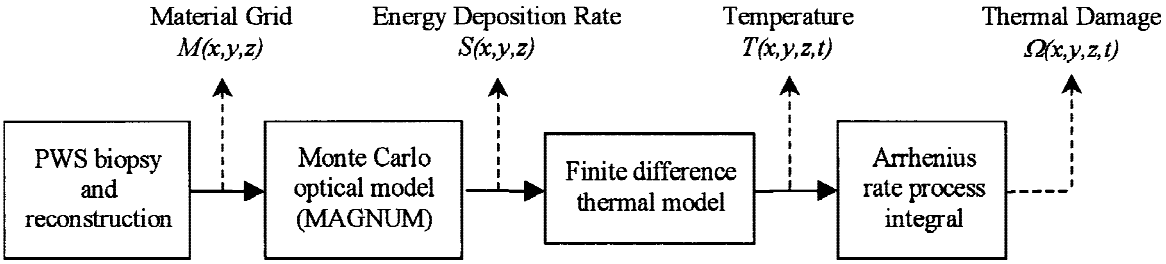

Fig. 1. Flow chart of the image-based optical-thermal modeling technique. Boxes represent processes or numerical algorithms and italics specify data matrices.

function of time and an exponential function of temperature [18,30,31].

Specification of Skin Anatomy

To ascertain the anatomy of vascular lesions, skin biopsies have been analyzed in different ways. Early studies involved techniques such as statistical analysis of vessel distribution and size from light microscopy evaluation of histology [32] and physical reconstruction involving microphotographs of tissue sections, string and glue [33]. Recently, noninvasive methods for optical biopsy, such as optical coherence tomography (OCT), have begun to show promise as potential sources for realistic Monte Carlo model geometries [24]. However, imaging of skin to the depth and quality necessary to produce clinically relevant simulation data is not possible with present technology.

The dependence of optimal laser parameters on dermal vasculature has been indicated by numerical [20] and clinical [34] studies. In a recent review article, van Gemert et al. concluded that future PWS treatment will incorporate "precise definition of the vascular anatomy...combined with laser parameters selected on an individual patient basis." [35].

Objective and Goals

The objective of this study was to develop a model that predicts energy deposition rate, temperature rise, and thermal damage based on a geometry derived from high-resolution images of a PWS and thus bring the vision of patient-specific determination of treatment parameters one step closer to clinical viability.

The specific goals of this study were (1) development and implementation of a novel optical-thermal numerical model; (2) reconstruction of a PWS biopsy into a three-dimensional matrix that can be incorporated into the model; and (3) simulation of PWS laser treatment using clinically relevant parameters including pulse durations of 0.5, 5.0, and 10.0 ms.

METHODS

An overview of the modeling process, which involved imaging and reconstruction of the PWS biopsy, optical simulation, heat transfer simulation, and thermal damage estimation, is shown in Figure 1.

PWS Biopsy and Computer Reconstruction

A complete description of the biopsy procedure and results was presented by Smithies et al. [36], whereas a brief summary is presented here. A portion of a light-purple superficial PWS from the forearm of a 30-year-old Caucasian female was excised, fixed, and then cut into 6 μm thick sections and stained with hematoxylin and eosin. A color video camera was used to record images of the individual sections. A commercial image-visualization package was used to define air, epidermis, dermis, and blood vessel regions and synthesize two-dimensional images into a three-dimensional tissue matrix. Each matrix entry, representing a 2 μm (x) × 6 μm (y) × 2 μm (z) rectangular voxel, was assigned an integer label according to tissue type [36].

For the present study, we have divided the original tissue grid (2 mm × 0.5 mm × 1 mm) into a smaller region and added a "cushion" of five voxels in the x and y directions so as to minimize the effect of boundary conditions on nearby blood vessels. The tissue grid implemented in the simulations presented here was comprised of 52 x-z sections, each containing 134 × 230 voxels (Fig. 2). Thus, a tissue volume with physical dimensions of (x,y,z) 268 μm × 312 μm × 460 μm was represented. For the tissue geometry shown in Figure 2, air and dermis are transparent, whereas the epidermis is shown in light gray and the blood

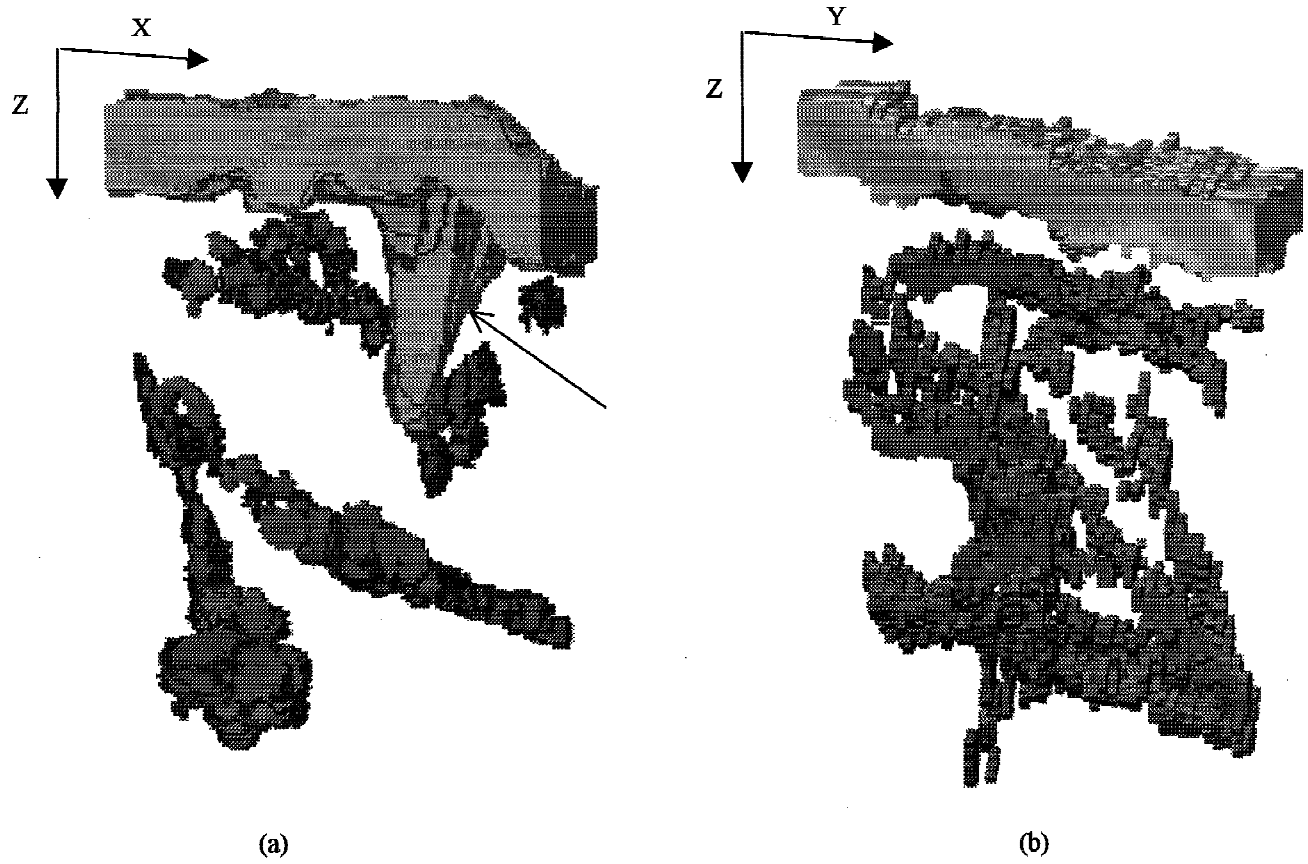

Fig. 2. Computer reconstruction of PWS biopsy region used in simulations. The illustrations show two sub-volumes of the material grid used in the simulations **(a)** an *x-z* section cut-away at $y = 29$ (29 of 52 slices in the *y* direction) and **(b)** a *y-z* section cut-away at $x = 31$ (31 of 133 slices in the *x* direction). These sections are used in subsequent figures. Air and dermal regions are transparent to improve visibility of PWS vasculature. Epidermis (top, lighter gray) and blood vessels (bottom, darker gray) are visible. Note the epidermal region surrounding a hair follicle which projects into the dermis (arrow).

vessels in dark gray. Figure 2 shows cut-aways of the tissue volume along *x-z* and *y-z* slices. The *x-z* slice included vessels and vessel clusters running perpendicularly to the section, whereas the *y-z* slice contained a branching vessel extending towards the epidermis.

Optical Model

MAGNUM is based on the weighted photon Monte Carlo technique in which a large number of single "photon packets" are propagated through the tissue and deposited in "bins" in the energy deposition matrix according to the locations where absorption events occur [14,37]. Stochastic relations are used to simulate the photon's random walk, which includes events such as absorption, scattering, reflection, and refraction. These relations incorporate optical properties, specifically, absorption coefficient (μ_a), scattering coefficient (μ_s), anisotropy (g), and index of refraction (n), of the tissue in which the photon propagates. As the number of photons launched and absorbed becomes large, the energy deposition matrix converges to a solution for distribution of absorbed energy. MAGNUM was developed through modification of the basic Monte Carlo light propagation technique so as to account for three-dimensional tissue structures with non-homogeneous optical properties [23]. The primary novelty of this model involves alteration of the path length of segments of the photon's random walk according to the optical properties of each voxel the photon passes through, in a manner similar to that used in layered Monte Carlo models.

Modification of MAGNUM was required to simulate irradiation of the PWS reconstruction presented here. Since the superficial surface of the tissue volume was much smaller than that covered by 5–10 mm diameter laser spot, the beam was approximated as being infinitely wide.

This was accomplished by distributing photon launch sites evenly across the tissue surface and employing totally internally reflective side boundaries. A 1 mm thick dermal sublayer was implemented in which the photon was allowed to propagate until returning to the material grid region or being absorbed or transmitted. The rate of energy deposition in the tissue volume was computed for a 1 W/cm^2 irradiance. This distribution was linearly scaled to account for specific irradiance levels, thus providing the heat source term (S) for the thermal model. Fluence rate was calculated by dividing the energy deposition rate in a voxel by the local absorption coefficient.

Thermal Model

After the distribution of energy deposition was found, the temperature rise in the tissue was computed. The Fourier heat conduction equation was employed instead of the bioheat equation [38] (which incorporates an additional perfusion term) for two reasons: (1) blood vessels were defined explicitly, rather than as a distributed source or sink in the tissue and (2) for the short pulse durations simulated in this study, thermal effects of blood perfusion are negligible [39]. The multidimensional, time-dependent form of this equation was employed so as to enable a transient solution for a tissue volume with realistic heterogeneity in thermal properties and energy deposition rate:

$$\rho c \frac{\partial T}{\partial t} = \frac{\partial}{\partial x}\left(k \frac{\partial T}{\partial x}\right) + \frac{\partial}{\partial y}\left(k \frac{\partial T}{\partial y}\right) + \frac{\partial}{\partial z}\left(k \frac{\partial T}{\partial z}\right) + S, \tag{1}$$

where T (°C) is temperature, t (seconds) is time, S (W/m^3) is the heat source term, ρ (kg/m^3) is density, c (J/kg/°C) is specific heat, and k (W/m/°C) is thermal conductivity [40]. The explicit finite difference (forward-difference) technique was used to discretize and numerically solve the heat conduction equation. Calculation of average thermal conductivity between voxels was performed by using a harmonic mean. Adiabatic boundary conditions were applied to the five internal tissue boundaries, whereas the standard convection condition was used to describe heat flow from superficial surface voxels to the air [41]:

$$-k \left.\frac{dT}{dz}\right|_{surface} = h(T_{air} - T_{surface}), \tag{2}$$

where $T_{surface}$ and T_{air} are the temperatures of the surface voxel and air, respectively, and h (W/m^2/°C) is the convection coefficient. The temperature distribution was solved explicitly using a large number of small time steps in order to maintain numerical stability, maximize solution accuracy, and document transient changes. The temperature matrix corresponded one-to-one with the material grid and energy deposition matrices. Thus, the control volume elements in the thermal model were of identical size as the bins in the optical model and the voxels in the tissue grid.

The pathological changes in biological tissue brought about by temperature rise were represented by the coefficient of thermal damage, Ω [30,31], which was evaluated using an Arrhenius rate process integral that assumed constant rate process coefficients:

$$\Omega(t) = A\int_0^t \exp\left[-\frac{E_a}{RT(\tau)}\right] d\tau, \tag{3}$$

where A (1/s) is the frequency factor or molecular collision rate, E_a (J/mole) is activation energy and R (8.314 J/mole/°K) is the universal gas constant. The thermal damage calculation was implemented as a subroutine in the thermal diffusion model. After the temperature distribution at a particular time step was calculated, the latest and next-to-latest temperatures, T(t) and T(t−Δt), were used to calculate the change in thermal damage for each voxel by using numerical integration by the trapezoidal method. Thermal simulations were continued until the tissue had cooled to 50 °C, a temperature at which the rate of thermal damage accumulation was insignificant. This typically occurred within tens of milliseconds of the end of the laser pulse.

Simplifications and Assumptions

As with any model, assumptions and simplifications were made. In focusing on the effect of realistic tissue geometry, consideration of various mechanisms was sacrificed. Although a recent study has produced important data on the temperature dependence of blood absorption at 586 nm [42], computational limitations precluded the incorporation of dynamic (temperature, pressure, thermal damage, or hydration-dependent) changes in optical and thermal properties. Owing to the short pulse durations considered, the role of blood fluid dynamics was neglected. Tissue geometry was specified with voxels that distorted the

TABLE 1. Optical Properties of Skin Components for λ = 585 nm [3].

	μ_a (cm^{-1})	μ_s (cm^{-1})	g	n
Epidermis	18	470	0.79	1.37
Dermis	2.4	129	0.79	1.37
Blood	191	467	0.99	1.33

TABLE 2. Thermal Properties of Skin Components [18].

	k (W/m/°C)	ρ (kg/m^3)	c (J/kg/°C)
Epidermis	0.21	1,200	3,600
Dermis	0.53	1,200	3,800
Blood	0.55	1,100	3,600

true shape of the tissue. The accuracy of these simulations is also limited by the use of an infinitely wide beam approximation and a homogeneous dermal sublayer.

Simulation Parameters and Conditions

Laser pulse duration was the primary independent variable in this study (0.5, 5, and 10 ms). The irradiances for these simulations were chosen so as to create a maximum temperature of 100°C in the tissue section in Figure 2a. This temperature level was chosen so as to generate thermal damage in and around the vessels.

The optical properties (absorption coefficient, μ_a, scattering coefficient, μ_s, anisotropy factor, g, and index of refraction, n) of skin for a laser wavelength of 585 nm are shown in Table 1. A single simulation using MAGNUM produced the energy deposition grid that was implemented, after appropriate linear scaling for irradiance, as the source term for the three thermal simulations.

The initial and environmental temperatures were assigned values of 37°C and 22°C, respectively. The convection coefficient (h) of 25 $W/m^2/°C$ corresponded to a condition of free convection (exposure to an air environment with minimal velocity). A time step of 2.5 μs was used so as to satisfy stability criteria. Thermal material properties used by Sturesson and Andersson-Engels [18], and found to be in reasonable agreement with data compiled by Duck [43], were employed in these simulations (Table 2). Thermal damage coefficients for skin ($A = 3.1 \times 10^{98}$ 1/s; $E_a = 6.27 \times 10^5$ J/mole) were taken from Henriques [44].

In order to identify the irradiance levels that resulted in a maximum tissue temperature of 100°C, the thermal model was performed iteratively until convergence within 1°C was reached. In all three simulations, the maximum temperature occurred in or near the large superficial vessel cluster (seen in Fig. 3a), although the exact location varied. The irradiances used in the three simulations reported here are displayed in Table 3.

RESULTS

Spatial and temporal distributions of deposited energy, temperature, and thermal damage are impossible to view in their entirety within the format constraints of this article. A three-dimensional perspective of the reconstructed tissue geometry and Monte Carlo simulation results for wavelengths of 532 and 585 nm may be viewed in an electronic journal via the world wide web [25]. The results and discussion presented here deal primarily with thermal mechanisms.

Graphical representations of energy deposition rate, temperature and thermal damage results are presented in two formats: as contour plots for slices corresponding to the *x-z* and *y-z* cut-aways in Figure 2a,b (Figs. 3–9) and line charts for data corresponding to the location of the vertical line in Figure 3a (see Fig. 10).

The distribution of energy deposition rate for an irradiance of 1 W/cm^2 is shown in Figure 3. Four regions are visible in Figure 3: air, epidermis, dermis, and blood vessels. The energy deposition rate in the blood vessels decreased from approximately 300 to 100 W/cm^3 due to attenuation with depth as well as shading effects. Values decreased (on average) from 40 to 33 W/cm^3 in the epidermis and from 4 to 1.5 W/cm^3 in the dermis, primarily as a function of depth.

Thermal modeling results showed a general trend from specific to nonspecific injury for increasing pulse duration (Fig. 4–9). Figures 4–6 display the temperature distributions at the end of the laser pulses. For $\tau_p = 0.5$ ms (Fig. 4a), temperature rise corresponded to energy deposition, although temperature was also a function of local blood concentration. For $\tau_p = 5$ and 10 ms (Figs. 5a, 6a), temperature rise in the blood became more dependent on tissue geometry than energy deposition rate, with temperatures above 90°C occurring in larger superficial as well as deep vessels or vessel clusters. Heat generated in the blood and epidermis had a greater amount of time to diffuse into the cooler dermis, leading to decreased temperature gradients and wider isotherms. The maximum temperatures in Figures 4a and 5a ($\tau_p = 0.5$, 5 ms) did not occur in the most superficial vessel, rather in one of the larger vessels of a shallow cluster.

Figures 7–9 document the distribution of thermal damage for each of the three pulse dura-

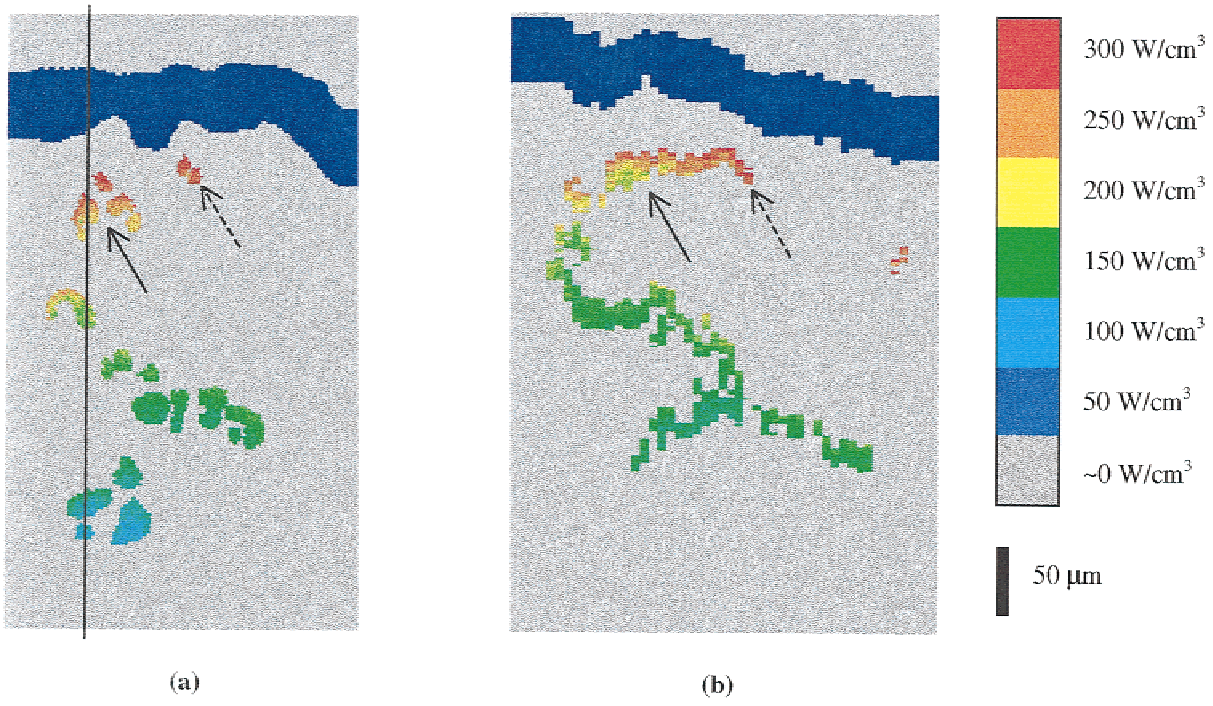

Fig. 3. Energy deposition rate in the **(a)** *x-z* and **(b)** *y-z* sections corresponding to the cutaways in Figure 2. Simulated laser parameters included an infinitely wide beam at $\lambda = 585$ nm with an irradiance of 1 W/cm^2. Solid vertical line denotes location of data presented in Figure 10. Solid and dashed arrows indicate large and small vessel structures referred to in the Discussion.

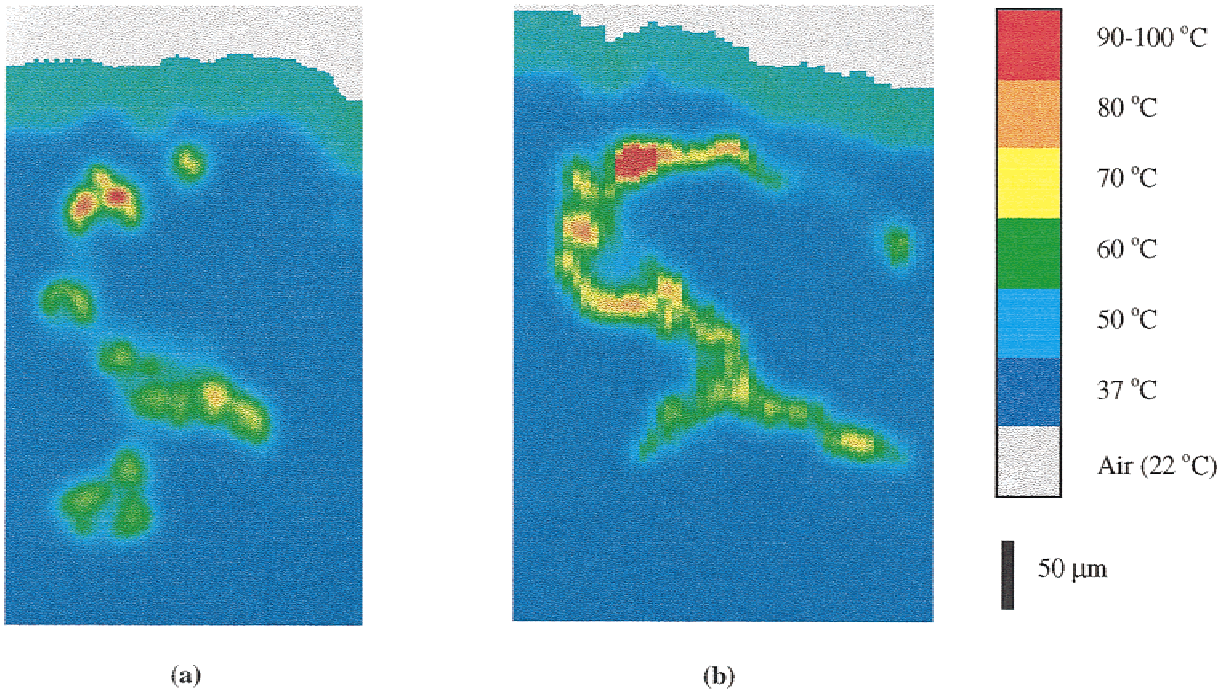

Fig. 4. Temperature distributions in the **(a)** *x-z* and **(b)** *y-z* sections at the end of the 0.5 ms laser pulse with irradiance (E) of 3660 W/cm^2 (radiant exposure, H = 1.8 J/cm^2).

TABLE 3. Irradiance/Radiant Exposure Levels for Thermal Simulations.

Pulse Duration (ms)	0.5	5.0	10.0
Irradiance (W/cm^2)	3660	980	670
Radiant Exposure (J/cm^2)	1.8	4.9	6.7

tions after the maximum tissue temperature relaxed to less than 50°C. Regions of native or minimally damaged tissue ($\Omega < 1.0$) are displayed in lighter shades whereas coagulated regions ($\Omega > 1.0$) are darkened. The shortest pulse duration created thermal damage to blood, with a preference for larger, superficial vessels (Fig. 7). Damage was generated towards the center of vessel clusters for the 5 ms pulse (Fig. 8), whereas the extent of damage in more isolated vessels was decreased. Epidermal coagulation was predicted for the two longest pulse durations. This damage region extended into the superficial region of the dermis for $\tau_p = 10$ ms (Fig. 9).

Figure 10a,b,c shows energy deposition (and fluence rate), temperature, and thermal damage results, respectively, as a function of depth in the skin. These figures provide a more quantitative assessment of the data presented in Figures 3–9. Note that "Depth" for Figure 10 is measured from the air/epidermis interface. The fluence and energy deposition rates shown in Figure 10a give an indication of the convergence level of the simulation, as well as the influence of shading effects inside and around blood vessels. Temperature distributions at the end of the laser pulse for each of the three simulations are graphed in Figure 10b, whereas Figure 10c indicates final levels of thermal damage (Ω).

DISCUSSION

The relationship between energy deposition and temperature rise is not a linear one. Therefore, knowledge of the distribution of absorbed energy is necessary but not sufficient for accurate prediction of vessel damage. The effectiveness of PWS laser treatment is determined in a large part by heat transfer mechanisms, which can be strongly influenced by variations in pulse duration and tissue structure.

Tissue Structure

In the study describing the PWS reconstruction [36], the authors suggested that the poor response of the PWS to laser treatment may be a result of optical and thermal mechanisms inherent in a network of small vessels containing numerous vessel clusters. Proximity of vessels to each other gave rise to a shading effect, a decrease in the energy deposited in a particular vessel because of the proximity of other vessels. The energy absorbed by the small capillaries was quickly conducted away, since the thermal relaxation time of these vessels was on the order of hundreds of microseconds. The simulations performed in this study were used to evaluate these suggestions.

The data demonstrated that vessels within a few microns of each other may produce a direct shading effect, particularly a decrease in energy deposition rate in vessels forming clusters. Such an effect has been predicted for 190 μm diameter vessels [23] and is due to the fact that light in the dermis is not isotropic, but has a depth-wise (positive z direction) directionality. Thus, size and proximity of vessels affect local energy deposition rate. Although a general decrease in fluence rate due to shading was not demonstrated explicitly, it likely had an effect corresponding to overall blood concentration in the skin [20].

The modeled results are in general agreement with previous studies which have demonstrated the relationship between vessel size and temperature rise [22,35]. Smaller vessels had shorter thermal relaxation times, which made them more resistant to heating and damage. In the most superficial portion of the y-z section, as the blood vessel approaches the epidermis its diameter decreases from about ~30 to ~20 μm (denoted by solid and dashed arrows, respectively, in Fig. 3a) and the average energy deposition rate in the vessel increased slightly. The temperature at the end of the laser pulse in the thinner region was less than that of the thicker region for all three pulse durations. This discrepancy in temperature rise was a result of differences in thermal mass and the fact that the volume to surface area ratio increases with vessel size, thus reducing the relative heat flow rate from the vessel to the dermis.

However, when small vessels are located in proximity to one another they produce a thermal effect that is similar to a single large vessel. An example of the difference between heating of an isolated vessel and a vessel cluster was seen in the superficial region of the x-z section (Figs. 3a, 4a, 5a, 6a). The small vessel (indicated by dashed arrow in Fig. 3a) absorbed similar levels of energy as the vessel cluster (solid arrow, Fig. 3a) yet had a

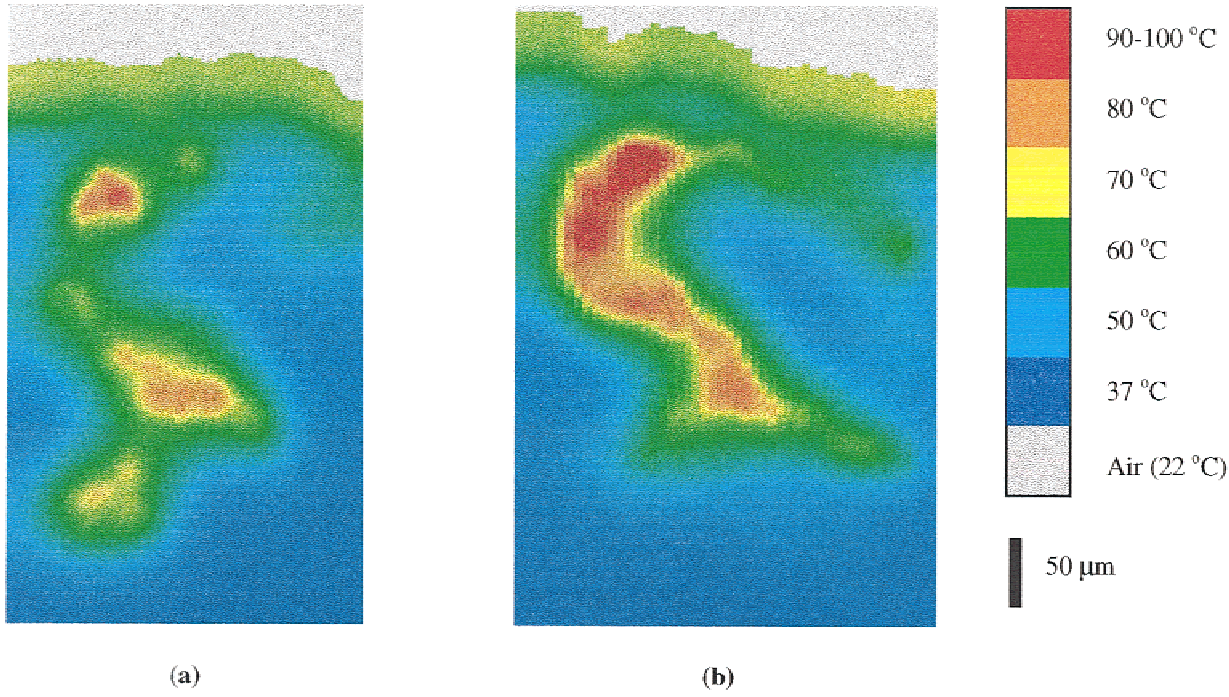

Fig. 5. Temperature distributions in the **(a)** *x-z* and **(b)** *y-z* sections at the end of the 5 ms laser pulse for E = 980 W/cm^2 (H = 4.9 J/cm^2).

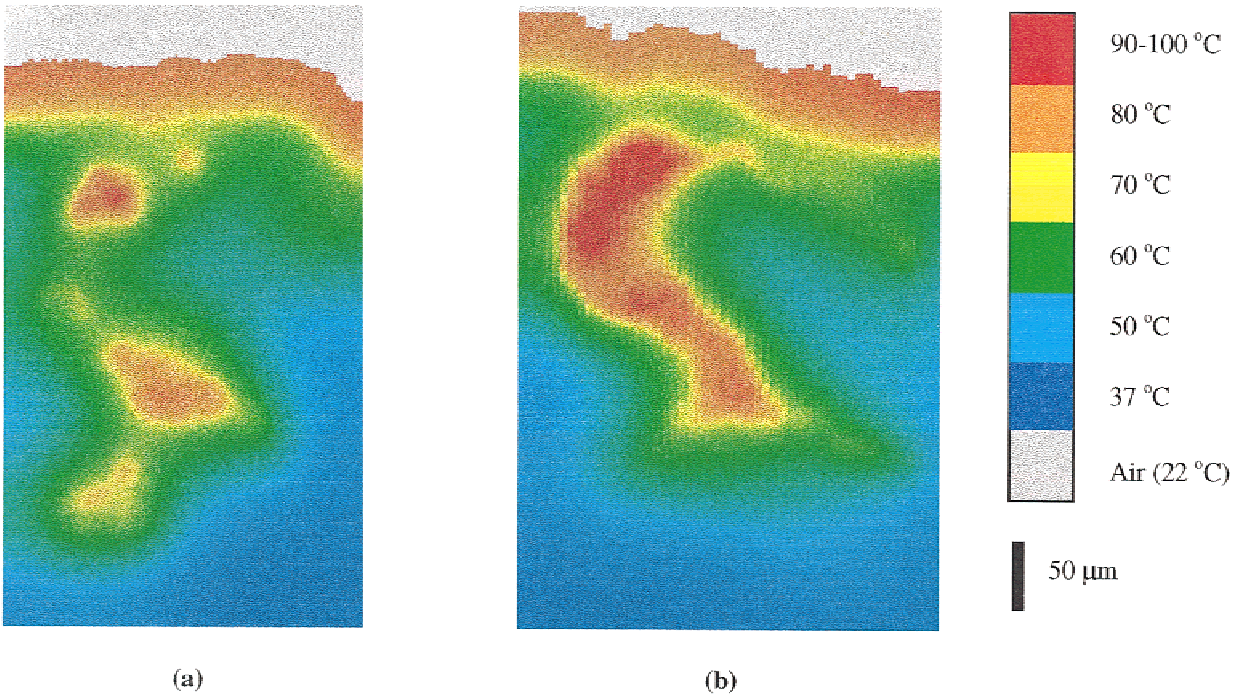

Fig. 6. Temperature distributions in the **(a)** *x-z* and **(b)** *y-z* sections at the end of the 10 ms laser pulse for E = 670 W/cm^2 (H = 6.7 J/cm^2).

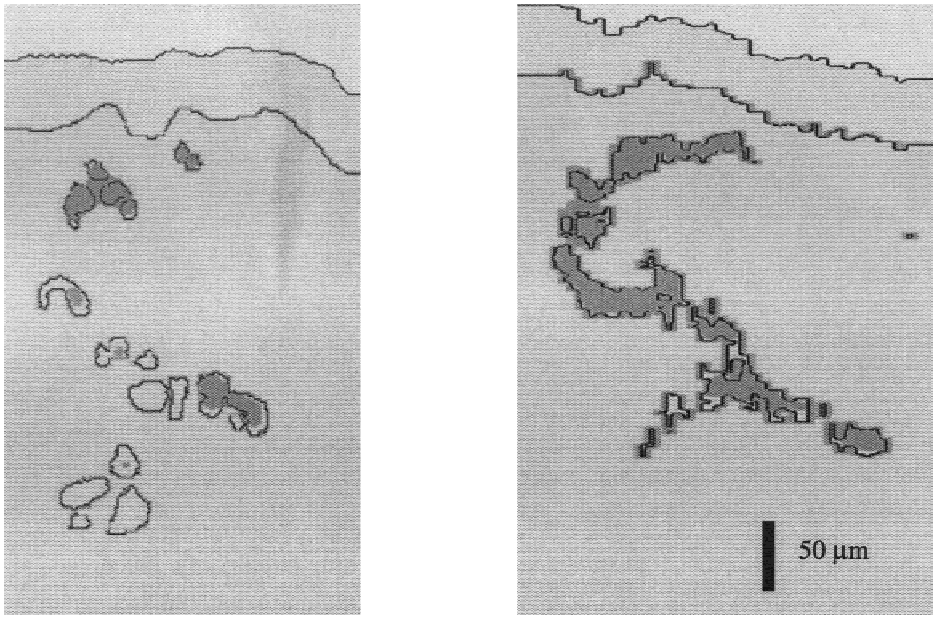

Fig. 7. Extent of thermal damage in the **(a)** *x-z* and **(b)** *y-z* sections for τ_p = 0.5 ms and E = 3,660 W/cm^2 (H = 1.8 J/cm^2). Shaded regions indicate coagulation ($\Omega > 1$). Black lines represent air-tissue and skin component boundaries. Damage is confined to blood vessels and superficial dermis between blood vessels.

lower temperature rise and level of thermal damage during each of the three laser simulations than corresponding structures in the vessel cluster. Rapid temperature rise in the dermis resulted from the accumulation of heat diffusion from surrounding vessels. As the dermis increased in temperature, energy absorbed in a vessel was not as easily conducted towards the center of the cluster due to the reduced temperature gradient. Thus, heat built up more rapidly and led to a region of increased temperature that included blood and dermis alike. These results indicate that thermal interaction of multiple vessels in close proximity, such as arteriole-venuole pairs, bifurcations, crossing vessels, and clusters, may alter the local accumulation of thermal damage.

Pulse Duration

Variations in the irradiance/radiant exposure required to attain a maximum temperature of 100 °C indicated the effect of heat conduction in the treatment of PWS. Data in Table 2 can be explained in either of two ways: 1) as pulse duration increased, heat had more time to diffuse away from regions of high energy deposition, thus greater radiant exposures were required to reach a specific temperature; or 2) as irradiance was decreased, a longer pulse was required to deliver sufficient energy to attain a specific temperature. Either way, the heating event becomes less confined and resulting damage less specific.

The simulation results indicated a high degree of thermal confinement for τ_p = 0.5 ms. Although some conduction occurred during the laser pulse, a double-peaked temperature rise was produced where vessel spacing was small (Fig. 10b at a depth of 325 μm). These results provide evidence that the thermal confinement time for small vessels (D ~ 25 μm) is on the order of 0.5 ms, which compares favorably with the range of values (0.25–0.61 ms) found using time constant analysis [45]. Although the pulse duration was, by formal definition, thermally confined, the heat conducted away from these small vessels during a 0.5 ms laser pulse was still enough to produce a notable reduction in temperature and thermal damage at the edge of the vessel. The lack of significant damage to the epidermis or dermis for the 0.5 ms case is in agreement with numerical [10,29] and clinical [4,46] studies.

The increase in pulse duration from 0.5 ms to 5 ms brought about significant changes in temperature and thermal damage distributions. Temperature distributions were more diffuse, wash-

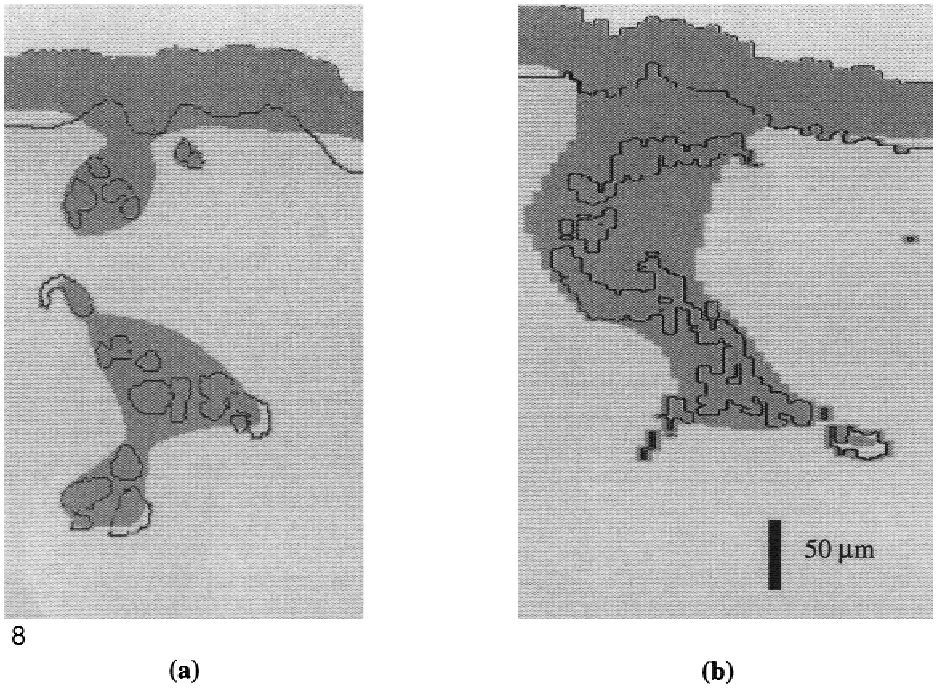

Fig. 8. Extent of thermal damage in the **(a)** *x-z* and **(b)** *y-z* sections for $\tau_p = 5$ ms and $E = 980$ W/cm^2 ($H = 4.9$ J/cm^2). Shaded regions indicate coagulation ($\Omega > 1$). Black lines represent air-tissue and skin component boundaries. Damage is confined to the epidermis, blood, and dermis around larger vascular structures.

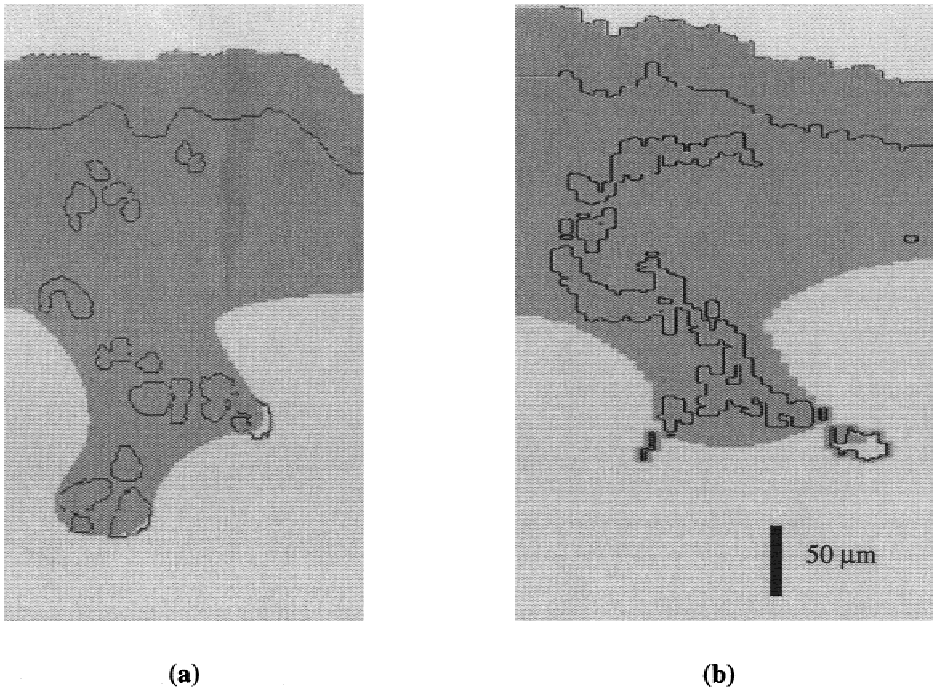

Fig. 9. Extent of thermal damage in the **(a)** *x-z* and **(b)** *y-z* sections for $\tau_p = 10$ ms and $E = 670$ W/cm^2 ($H = 6.7$ J/cm^2). Shaded regions indicate coagulation ($\Omega > 1$). Black lines represent air-tissue and skin component boundaries. Widespread damage extends from the epidermis throughout most of the superficial regions of the skin and in wide perivascular regions. The only native blood regions are in deeper vessels towards the edge of clusters.

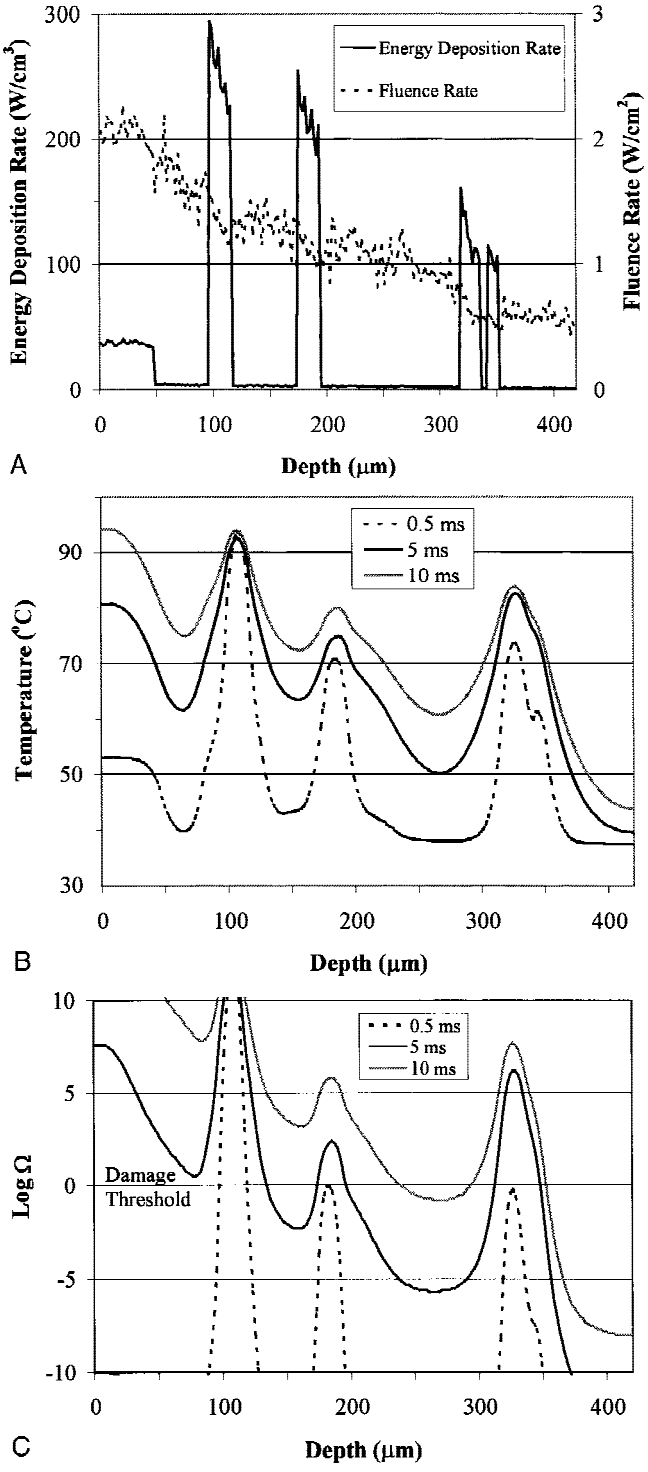

Fig. 10 **a:** Energy deposition and fluence rates in port wine stain skin for an "infinitely wide" beam with an irradiance of 1 W/cm^2 at λ = 585 nm. The data in Figure 10**a–c** correspond to the location of the vertical line in Figure 3. Energy deposition data correspond to data in Figure 4a. **b:** Temperature distributions at the end of 0.5, 5, and 10 ms laser pulses correspond to data in Figures 4a, 5a, and 6a. Partial thermal confinement is indicated in the epidermis by maximum temperatures directly proportional to radiant exposure and in the blood for the 0.5 ms pulse as a double-peaked temperature rise corresponding to the two deepest vessels. **c:** Final levels of thermal damage after maximum tissue temperature returned to 50°C, shown as the logarithm of the thermal damage coefficient, Ω. Corresponds to data in Figures 7a, 8a, and 9a. Threshold damage level is Ω = 1. Progression from selective to perivascular to nonselective damage is seen with increasing pulse durations.

ing out features such as the double-peaked temperature rise mentioned above. Maximum temperatures became more a function of the size of vessel structures than local energy deposition rates. An increase in the significance of the effect mentioned above, where small, isolated vessels exhibit reduced temperatures as compared to larger vessel structures was seen. Significant perivascular damage was predicted for larger vessel structures. These results are in qualitative agreement with previous numerical modeling results [12,22,29].

The τ_p = 10 ms simulation indicated increased temperature and widespread damage throughout superficial regions of the tissue volume as well as in and around larger deep blood vessels. Isotherms became smoother and the tissue geometry continued to increase in significance over energy deposition rate in determining temperature rise, as compared to τ_p = 5 ms. The results for the τ_p = 10 ms simulation are in general qualitative agreement with long pulse duration clinical studies: KTP laser irradiation (λ = 532 nm, τ_p = 10 ms) with surface cooling resulted in damage to perivascular collagen [47] and argon laser irradiation (λ = 488, 514 nm, τ_p = 200–400 ms) produced widespread damage to the superficial dermis [48]. It should be noted, however, that epidermal absorption is higher at these wavelengths than at 585 nm.

Energy absorbed in the epidermis exhibited thermal confinement for τ_p = 0.5 ms and to some extent for τ_p = 5 ms. Thus, the temperature rise was proportional to radiant exposure. Conduction from the epidermis began to become significant for τ_p = 5 ms, resulting in an increase in thermal damage to dermal regions which were subjected to heat diffusing from both the epidermis and blood vessels. For τ_p = 10 ms, maximum epidermal temperatures approached the maximum temperatures produced in the blood vessels. Heat diffusing from the epidermis to the dermis combined with energy absorbed in superficial blood vessels to cause extensive, nonselective damage throughout much of the superficial portion of the skin.

Threshold Temperatures for Thermal Damage

For τ_p = 0.5 ms, the predicted coagulation (Ω>1) extent corresponded to the isotherm of 70°C (Fig. 4a) for vessels which had maximum temperatures greater than 70°C and were thus able to keep a region of tissue heated for sufficient time. Some deeper and smaller blood vessels reached 70°C but did not remain at this temperature long enough to induce thermal damage. Thermal damage for the 5 ms laser pulse occurred above temperatures of approximately 70°C, although correlation to the isotherms was not exact due to the transient, geometry-dependent nature of the temperature distribution and the time-temperature nature of thermal damage accumulation. For τ_p = 10 ms, prediction of coagulation extent is more closely correlated to the 60°C isotherm than the 70°C isotherm, due to the increased exposure duration.

Optimal PWS Treatment Parameters

Before modeling can be used to accurately determine the optimal laser parameters for treatment of PWS, the relationships between specific thermal endpoints and clinical outcomes need to be more thoroughly established. The primary indicators of non-ablative photothermolysis are vessel wall coagulation and vessel blockage by blood coagulum formation [4]. However, numerous questions remain unanswered, such as: What extent of blood coagulation or vessel wall denaturation is necessary to create necrosis as opposed to recoverable occlusion or embolized coaguli? [6,49]. What is the relative heat stability of skin constitutents? [46]. What extent of epidermal or dermal damage creates undesired results such as hyper- and hypo- pigmentation and scarring? [48]. What levels of energy deposition/temperature rise produce vaporization of blood and mechanical vessel wall damage? For the purpose of this study, we assume that coagulation of blood and a thin layer of dermis corresponding to the vessel wall is sufficient for successful treatment, and that extensive dermal or epidermal damage causes an undesirable result.

In the three simulations performed, the resulting thermal damage distributions did not indicate optimal treatment of the PWS lesion. For τ_p = 0.5 ms, most coagulated regions were confined to blood vessels, often filling the entire lumen. Higher irradiances at the same pulse duration would likely result in increased perivascular coagulation [50]; however, maximum temperatures in excess of 100°C would be generated. For longer pulse durations, temperatures in the dermis and epidermis exceeded the threshold for coagulation. Therefore, the optimal pulse duration for this PWS geometry most likely lies between 0.5 ms and 5 ms, corresponding to a regime where heat diffusion is significant enough to damage vessel walls without producing large volumes of necrotic epidermis and dermis.

The depth of predicted coagulation of blood vessels (<300 μm) is much smaller than has been achieved experimentally at λ = 585 nm (1.16 mm for radiant exposures of 6–7 J/cm^2) [4]. Simulation of clinical radiant exposure levels would likely result in the generation of high temperatures in the epidermis and superficial vessels. Although temperatures above 100°C are generally expected to produce blood vaporization and vessel hemorrhage [50], threshold temperatures for laser-induced ablative phase change have not been established experimentally. Epidermal damage is a common side effect of laser treatment; however, effective surface cooling techniques [47,51,52] can be used to induce deep vascular damage, while sparing the epidermis. Skin cooling may be especially effective in reducing or eliminating the superficial damage created during long laser pulses.

Tissue Representation

Computer reconstruction of a PWS biopsy enabled specification of a realistic geometry for simulation of laser treatment. The tissue matrix used for these simulations required more than 1.6 million voxels. As seen in Figure 2, specification of the tissue sections with 2 μm resolution (x-z planes) provided well-defined surfaces. Owing to limitations associated with histological processing, the resolution perpendicular to the sections (along the y axis) was limited to 6 μm, resulting in discontinuities in the epidermis and blood vessels. Physical movement of the tissue components during sectioning may have contributed to irregularities in the shape of the small blood vessels. Additionally, specification of a blood vessel with voxels that are larger than a tenth of its diameter will likely result in boundaries which appear irregular.

Inaccurate specification of tissue anatomy can lead to poor results from optical and thermal models. If a vessel is misaligned in the material matrix, then more photons propagate into the ves-

sel center, leading to an over-prediction of energy deposition rate. Misalignment also leads to an increase of vessel surface area, and thus an overestimation of heat loss from the vessel by the thermal model. Given the difficulties of handling such thin tissue sections, an improvement in the quality of tissue grids from histological sources seems unlikely. However, improvements in geometry specification may be achieved by implementing smoothing and/or vessel tracing routines in which the vessels are specified as curves in three-dimensional space before being converted into a three-dimensional grid [23].

Boundary Conditions

The 10 ms laser pulse was long enough for heat generated in the epidermis and blood to diffuse extensively. The free convection surface boundary condition provided no noticeable cooling in this or other simulations. The insulating effect of air helped to contain the heat generated in the epidermis and superficial vessels to the superficial regions of the skin. Effective surface cooling would likely reduce or prevent thermal damage in the epidermis and superficial dermis.

Selection of an adiabatic condition for the five internal boundaries can result in an overestimation of temperature rise near blood vessels along the edge of the volume [53]. In order to minimize the effect of these thermal mirror-like boundary conditions a thin region of dermis was added along the edge of the tissue. As a result, the boundary conditions have little effect on temperature rise in the tissue, except for the longest pulse duration. A slight influence of the boundary condition, however, does not necessarily indicate a defect in the model, since in reality the tissue volume would be affected by heated tissue in adjacent regions.

Computational Considerations

The computational requirements for this study were significant, and may be prohibitively great for many computer systems. All simulations were performed on an IBM RS/6000 workstation. MAGNUM was run using 15 million photons, which required about 80 hours of processor time and two matrices (material grid, energy deposition) of approximately 1.6 million four-byte elements each. The thermal simulations required four matrices (material grid, energy deposition, temperature, and thermal damage) of 1.6 million four-byte elements each and processor times on the order of 30 minutes. Future improvements in memory size and processor speed will certainly facilitate simulation of larger tissue regions with increased accuracy and speed.

CONCLUSIONS

The numerical model presented here provides a new perspective on mechanisms observed in the results of simpler models yet is in general agreement with previous results in regards to trends in energy deposition, temperature rise and vessel destruction. By tomographically reconstructing a PWS biopsy and incorporating it in a novel optical-thermal model, we have provided a more accurate assessment of the effect of pulse duration on temperature rise and thermal damage in skin than was previously possible. Results indicated for a laser wavelength of 585 nm, a large beam diameter (5–10 mm) and the tissue geometry specified, the optimal pulse duration is in the range of 0.5 to 5 ms. The model predicted that increased vessel size and decreased separation of vessels would increase the extent of vascular and perivascular coagulation. The role of vasculature and the influence of epidermal heating were highly dependent on the decreasing thermal confinement that results from increased pulse duration. Future study of optimization of PWS treatment (such as investigation of epidermal cooling techniques) and other therapeutic laser procedures should help to clarify the theoretical and clinical significance of image-based, patient-specific approaches to simulation of laser-tissue interactions.

REFERENCES

1. Mulliken JB. The classification of vascular birthmarks. In: Tan OT, editor. Management and treatment of benign cutaneous vascular lesions. Philadelphia: Lea & Febiger. 1992.
2. Anderson RR. Laser-tissue interactions. In: Goldman MP, Fitzpatrick RE, editors. Cutaneous laser surgery: the art and science of selective photothermolysis. St. Louis: Magby. 1994.
3. van Gemert MJC, Welch AJ, Pickering JW, Tan OT. Laser treatment of port wine stains. In: Welch AJ, van Gemert MJC, editors. Optical-thermal response of laser-irradiated tissue. New York: Plenum Press. 1995.
4. Tan OT, Morrison P, Kurban AK. 585 nm for the treatment of Port Wine Stains. Plast Recon Surg 1990; 86: 1111–1117.
5. Kauvar ANB. Long-pulse, high energy pulsed dye laser treatment of port wine stains and hemangiomas. Lasers Surg Med 1997;Supplement 9:36.
6. van Gemert MJC, Welch AJ, Miller ID, Tan OT. Can physical modeling lead to an optimal laser treatment

strategy for port-wine stains? In: Wolbarsht ML, editor. Laser applications in medicine and biology. New York: Plenum Press. 1991.
7. Pickering JW, van Gemert MJC. 585 nm for the laser treatment of port wine stains: a possible mechanism. Lasers Surg Med 1991;11:616–618.
8. van Gemert MJC, Welch AJ, Pickering JW, Tan OT, Gijsbers GHM. Wavelengths for laser treatment of port wine stains and telangiectasia. Lasers Surg Med 1995; 16:147–155.
9. Keijzer M, Pickering JW, van Gemert MJC. Laser beam diameter for port wine stain treatment. Lasers Surg Med 1991;11:601–605.
10. Pickering JW, Butler PH, Ring BJ, Walker EP. Computed temperature distributions around ectatic capillaries exposed to yellow (578 nm) laser light. Phys Med Biol 1989;34:1247–1258.
11. van Gemert MJC, Pickering JW, Welch AJ. Modeling laser treatment of port-wine stains. In: Tan OT, editor. Management and treatment of benign cutaneous vascular lesions. Philadelphia: Lea & Febiger. 1992.
12. Dierickx CC, Casparian JM, Venugopalan V, Farinelli WA, Anderson RR. Thermal relaxation of port-wine stain vessels probed in vivo: the need for 1-10-millisecond laser pulse treatment. J Invest Dermatol 1995;105:709–714.
13. Anderson RR, Parrish JA. Microvasculature can be selectively damaged using dye lasers: a basic theory and experimental evidence in human skin. Las Med Sci 1981;1: 263–276.
14. Jacques SL, Wang L. Monte Carlo modeling of light transport in tissues. In: Welch AJ, van Gemert MJC, editors. Optical-thermal response of laser-irradiated tissue. New York: Plenum Press. 1995.
15. Verkruysse W, Lucassen GW, de Boer JF, Smithies DJ, Nelson JS, van Gemert MJC. Modelling light distributions of homogeneous versus discrete absorbers in light irradiated turbid media. Phys Med Biol 1997;42:51–65.
16. Miller ID, Veitch AR. Optical modelling of light distributions in skin tissue following laser irradiation. Lasers Surg Med 1993;13:565–571.
17. Verkruysse W, Pickering JW, Beek JF, Keijzer M, van Gemert MJC. Modeling the effect of wavelength on the pulsed dye laser treatment of port wine stains. Appl Opt 1993;32:393–398.
18. Sturesson C, Andersson-Engels S. Mathematical modelling of dynamic cooling and pre-heating used to increase the depth of selective damage to blood vessels in laser treatment of port wine stains. Phys Med Biol 1996;41: 413–428.
19. Keijzer M, Jacques SL, Prahl SA, Welch AJ. Light distributions in artery tissue: Monte Carlo simulations for finite-diameter laser beams. Lasers Surg Med 1989;9:148–154.
20. Smithies DJ, Butler PH. Modelling the distribution of laser light in port-wine stains with the Monte Carlo method. Phys Med Biol 1995;40:701–731.
21. Lucassen GW, Verkruysse W, Keijzer M, van Gemert MJC. Light distributions in a port wine stain model containing multiple cylindrical and curved blood vessels. Lasers Surg Med 1996;18:345–357.
22. de Boer JF, Lucassen GW, Verkruysse W, van Gemert MJC. Thermolysis of port-wine-stain blood vessels: diameter of a damaged blood vessel depends on the laser pulse length. Las Med Sci 1996;11:177–180.
23. Pfefer TJ, Barton JK, Chan EK, Ducros MG, Sorg BS, Milner TE, Nelson JS, Welch AJ. A three dimensional modular adaptable grid numerical model for light propagation during laser irradiation of skin tissue. IEEE J Sel Topics in Quantum Electron 1996;2:934–942.
24. Barton JK, Milner TE, Pfefer TJ, Nelson JS, Welch AJ. Optical low-coherence reflectometry to enhance Monte Carlo modeling of skin. J Biomed Optics 1997;2:226–234.
25. Barton JK, Pfefer TJ, Welch AJ, Smithies DJ, Nelson JS, van Gemert MJC. Optical Monte Carlo modeling of a true port wine stain anatomy. Optics Express (http://epubs.osa.org/opticsexpress/) 1998;2:391–396.
26. Rastegar S, Kim B, Jacques SL. Role of temperature dependence of optical properties in laser irradiation of biological tissue. Proc. SPIE 1992;1646:228–231.
27. Hielscher AH, Alcouffe RE, Barbour RL. Transport and diffusion calculations on MRI-generated data. Proc SPIE 1997;2979:500–508.
28. Svaasand LO, Fiskerstrand EJ, Kopstad G, Norvang LT, Svaasand EK, Nelson JS, Berns MW. Therapeutic response during pulsed laser treatment of port wine stains: dependence on vessel diameter and depth in dermis. Las Med Sci 1995;10:235–243.
29. Smithies DJ, Butler PH, Day WA, Walker EP. The effect of the illumination time when treating port-wine stains. Las Med Sci 1995;10:93–104.
30. Moritz AR, Henriques FC, Jr. Studies in thermal injury II. The relative importance of time and surface temperature in the causation of cutaneous burns. Am J Pathol 1947;23:695–720.
31. Pearce J, Thomsen S. Rate process analysis of thermal damage. In: Welch AJ, van Gemert MJC, editors. Optical-thermal response of laser-irradiated tissue. New York: Plenum Press. 1995.
32. Barsky SH, Rosen S, Greer DE, Noe JM. The nature and evolution of port wine stains: a computer-assisted study. J Invest Dermatol 1980;74:154–157.
33. Braverman IM, Keh-Yen A. Ultrastructure and three-dimensional reconstruction of several macular and papular telangiectases. J Invest Dermatol 1983;81:489–497.
34. Noe JM, Barsky SH, Geer DE, Rosen S. Port wine stains and the response to argon laser therapy: successful treatment and the predictive role of color, age, and biopsy. Plastic Reconstr Surg 1980;65:130–136.
35. van Gemert MJC, Nelson JS, Milner TE, Smithies DJ, Verkruysse W, de Boer JF, Lucassen GW, Goodman DM, Tanenbaum BS, Norvang LT, Svaasand LO. Noninvasive determination of port wine stain anatomy and physiology for optimal laser treatment strategies. Phys Med Biol 1997;42:937–950.
36. Smithies DJ, van Gemert MJC, Hansen MK, Milner TE, Nelson JS. Three-dimensional reconstruction of port wine stain vascular anatomy from serial histological sections. Phys Med Biol 1997;42:1843–1847.
37. Wang L, Jacques SL, Zheng L. MCML - Monte Carlo modeling of light transport in multi-layered tissues. Comp Methods Prog Biomed 1995;47:131–146.
38. Sturesson C, Andersson-Engels S. A mathematical model for predicting the temperature distribution in laser-induced hyperthermia: experimental evaluation and applications. Phys Med Biol 1995;40:2037–2052.
39. Welch AJ, Wissler EH, Priebe LA. Significance of blood flow in calculations of temperature in laser irradiated tissue. IEEE Trans Biomed Eng 1980;27:164–166.

40. Gebhart B. Heat conduction and mass diffusion. New York. McGraw-Hill. 1993.
41. Incropera FP, DeWitt DP. Fundamentals of heat and mass transfer. New York: John Wiley & Sons. 1985.
42. Verkruysse W, Nilsson AMK, Milner TE, Beek JF, Lucassen GW, van Gemert MJC. Optical absorption of blood depends on temperature during a 0.5 ms laser pulse at 586 nm. Photochem Photobiol 1998;67:276–281.
43. Duck FA. Thermal properties of tissue. In: Physical properties of tissue. London: Academic Press. 1990.
44. Henriques FC, Jr. Studies in thermal injury V. The predictability and significance of thermally induced rate processes leading to irreversible epidermal injury. Arch Pathol 1947;43:489–502.
45. van Gemert MJC, Welch AJ. Approximate solutions for heat conduction. In: Welch AJ, van Gemert MJC, editors. Optical-thermal response of laser-irradiated tissue. New York: Plenum Press. 1995.
46. Garden JM, Tan OT, Kerschmann R, Boll J, Furumoto H, Anderson RR, Parrish JA. Effect of dye laser pulse duration on selective cutaneous vascular injury. J Invest Dermatol 1986;87:653–657.
47. Adrian RM, Tanghetti EA. Long pulse 532-nm laser treatment of facial telangiectasia. J Invest Dermatol 1998;24:71–74.
48. Apfelberg DB, Maser MR, Lash J, Rivers JL. Progress report on extended clinical use of the argon laser for cutaneous lesions. Lasers Surg Med 1980;1:71–83.
49. Barton JK, Hammer DX, Pfefer TJ, Lund DJ, Stuck BE, Welch AJ. Simultaneous irradiation and imaging of blood vessels during pulsed laser delivery. Lasers Surg Med in press.
50. Tan OT, S. Murray, A.K. Kurban. Action spectrum of vascular specific injury using pulsed irradiation. J Invest Dermatol 1989;92:868–871.
51. Welch AJ, Motamedi M, Gonzalez A. Evaluation of cooling techniques for the protection of the epidermis during Nd-YAG laser irradiation of the skin. In: Joffe SN, editor. Neodymium-YAG laser in medicine and surgery. Amsterdam: Elsevier. 1983.
52. Anvari BH, Milner TE, Tanenbaum BS, Kimel S, Svaasand LO, Nelson JS. Dynamic epidermal cooling in conjunction with laser treatment of port-wine stains: theoretical and preliminary clinical evaluations. Las Med Sci 1995;10:105–112.
53. Pfefer TJ, Barton JK, Smithies DJ, Milner TE, van Gemert MJC, Nelson JS, Welch AJ. Laser treatment of port wine stains: three-dimensional simulation using biopsy-defined geometry in an optical-thermal model. Proc SPIE 1998;3245:322–333.